Spectrochimica Acta Part A: Molecular and Biomolecular Spectroscopy 142 (2015) 150–158

Contents lists available at ScienceDirect

Spectrochimica Acta Part A: Molecular and Biomolecular Spectroscopy

journal homepage: www.elsevier.com/locate/saa

Deconvolution procedure of the UV–vis spectra. A powerful tool for the estimation of the binding of a model drug to specific solubilisation loci of bio-compatible aqueous surfactant-forming micelle

Ilaria Calabrese [a], Marcello Merli [b], Maria Liria Turco Liveri [a,*]

[a] Dipartimento di Fisica e Chimica, Università degli Studi di Palermo, Viale delle Scienze – Parco d'Orleans II – Pad. 17, 90128 Palermo, Italy
[b] Dipartimento di Scienze della Terra e del Mare (DiSTeM), Università degli Studi di Palermo, Via Archirafi 36, 90123 Palermo, Italy

HIGHLIGHTS

- Successful non-conventional analysis of Nile Red/Tween 20 UV–vis-spectra evolution.
- Extended two pseudo-phases-model provides more precise and reliable Nile Red bindings.
- Spectra deconvolution allows Nile Red binding to specific micellar loci determination.
- Local binding mean values perfectly match with the classically evaluated ones.
- Drug confinement makes Tween 20 aggregates good candidates for modified drug delivery.

GRAPHICAL ABSTRACT

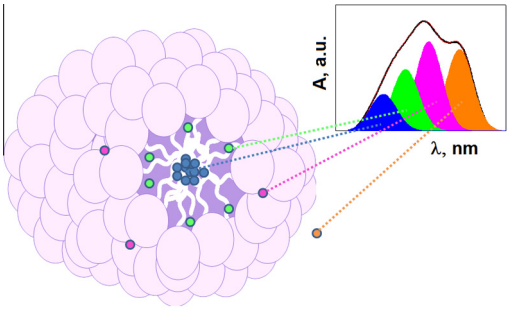

ARTICLE INFO

Article history:
Received 24 July 2014
Received in revised form 15 December 2014
Accepted 26 December 2014
Available online 20 January 2015

Keywords:
Nile Red
Tween 20
cmc
Deconvolution
Specific solubilisation *loci*
UV–vis spectra

ABSTRACT

UV–vis-spectra evolution of Nile Red loaded into Tween 20 micelles with pH and [Tween 20] have been analysed in a non-conventional manner by exploiting the deconvolution method. The number of buried sub-bands has been found to depend on both pH and bio-surfactant concentration, whose positions have been associated to Nile Red confined in aqueous solution and in the three micellar solubilisation sites. For the first time, by using an extended classical two-pseudo-phases-model, the robust treatment of the spectrophotometric data allows the estimation of Nile Red binding constant to the available loci. Hosting capability towards Nile Red is exalted by the pH enhancement. Comparison between binding constant values classically evaluated and those estimated by the deconvolution protocol unveiled that overall binding values perfectly match with the mean values of the local binding sites. This result suggests that deconvolution procedure provides more precise and reliable values, which are more representative of drug confinement.

Introduction

Our research group within a wide research project is aimed at "designing and *in-vitro*/*in-vivo* testing *ad hoc* carriers for biotechnological application". Very recently we have gauged the capability of a nanocomposite based on montmorillonite clay to deliver the antibiotic metronidazole [1]. Interestingly, the use of the new-tailor made formulation revealed to be very promising for prolonging the action of drug in the desired action site and also reducing both time and costs of preparation. In order to improve the performance of the nano-carriers either for the delivery of hydrophilic or

* Corresponding author. Tel.: +39 091 23898970; fax: +39 091 590015.
E-mail address: marialiria.turcoliveri@unipa.it (M.L. Turco Liveri).

http://dx.doi.org/10.1016/j.saa.2014.12.095
1386-1425/

hydrophobic drugs we have thought to functionalise the clay with surfactants.

Among the plethora of both synthetic and natural existing surfactants the polysorbates 20 (PS 20, also known as Tween 20 or TW 20) has been chosen. TW 20 has attracted the interest of both the scientific community and the biotechnology industry. This nonionic surfactant has been accepted from the World Health Organization (WHO) for its non-toxicity and biocompatibility which allows it to be used (above all) in pharmacological applications.

Polysorbates are amphiphilic, nonionic surfactants composed of two parts, i.e., the polar head group, polyoxyethylene sorbitan (POE sorbitan), and the hydrophobic ester tail.

Solutions of polysorbate 20 sold by manufacturers are chemically diverse mixtures of different fatty acid esters [2] and while the number of repeating ethylene oxide subunits varies at each position their total number ($w + x + y + z$) equals 20 and is constant for each polysorbate. The fatty acid moieties are attached through an ester linkage to the ethylene oxide oxygen at the z position. The laurate moiety of polysorbate 20 is a straight chain hydrocarbon structure. The prevalent use of the PSs is due to their high HLB (hydrophile–lypophile balance) numbers, low critical micelle concentration (cmc) values, and thus very efficient surface activity at low concentrations. Depending on the polysorbate concentration and solution conditions, i.e., temperature, sonication process, presence of additives (amphiphiles, electrolyte, other oil, etc.) these surfactants are able to self-organise into different types of nanostructures, namely spherical micelles, rods micelles, vesicles, oil-in-water emulsion, and so on. Analogously to the other surfactants, due to the dual nature of the amphiphilic molecules when the polysorbate is solubilised in water, as the tendency of the hydrocarbon chain of the surfactant is to minimise water contact, the monomers self-associate into micelles. These aggregates of the polysorbates with the ethylene oxide subunits protruded towards the aqueous surrounding solution and the hydrocarbon tails in the centre away from the water are thermodynamically stable. The interior properties of the micelles are similar to those of liquid hydrocarbon. The micelles are characterised by three preferential solubilisation sites, namely the polar head group (HG), the palisate layer (P) and the micellar core (C). Thus, the nature of the additive dictates the solubilisation locus in the different region of the micelle. In fact, hydrophilic species will be found in the polar head groups and palisade layer, amphiphilic molecules will be confined in solubilisation loci which depends on the nature and interaction involved in the uptake of the amphiphile. In particular, the solubilised can be found either in the polar head groups and the palisade layer, or in the palisade layer and the hydrophobic core; whereas the sparingly water soluble compounds privilege the hydrophobic interior. As a result, the nanostructured aggregates are able to significantly enhance the aqueous solubility of the insoluble compounds.

Bearing in mind these considerations both the designing and application of new tailor-made nano-carries based on clay/surfactant need, first of all, to establish both the capability of the "surface modifier" TW20 to self-aggregates and the stability of the blank self-organised aggregated under different pH conditions, i.e., those simulating the oral administration, the transdermal delivery, and so on. In addition, not only the stability of either the blank or the drug-loaded micelles is a requisite to which the nanostructured system has to obey but also the solubilisation locus of the drug into the micelle plays a relevant role.

For these reasons, we have investigated the physico-chemical behaviour of both the blank- and loaded-micelles, over a wide pH range from 1.0 to 7.4, in the submicellar and micellar concentration regions. The choice of this pH range was dictated by the pH condition experienced by a drug in physiological administration conditions. In particular, as it has been reported [3], when a drug, either in the free form or in a loaded nanostructure, is oral administrated it undergoes a pH gradient. Thus, the self-aggregation behaviour of the polysorbitan surfactant TW20 and its stability in aqueous solutions, under the experimental conditions used in the present work, have been established by performing surface tension and spectrophotometric measurements, respectively. In addition, the systematic spectrophotometric study allowed us to ascertain the stability of the drug-loaded micelles and the data treatment in a non-conventional way, i.e., by applying the deconvolution method, enabled us to estimate the binding constant of the NR to the specific solubilisation sites, namely the HG, the P and the hydrophobic C. For the sake of comparison the binding constant has been also evaluated by applying the classical procedure.

Classically, the binding constant of a probe [4,5], being different hydrophilicity, to micellar aggregates is estimated applying the two-pseudo phases model by considering only the change in the absorbance at the λ_{max} as a function of surfactant concentration. This situation mainly represents the palisade layer of the micelles where the solubilisation of the probe is governed by both the hydrophilic and hydrophobic interactions. However, in our opinion it cannot be leaved out of consideration that, depending on the nature of the probe, the other two solubilisation sites are involved in the drug-hosting. Bearing in mind these concerns and, to the best of our knowledge, the lack of binding data in the different solubilisation loci we have thought that the mathematical treatment of the spectrophotometric data by means of the deconvolution would give fruitful information since the solubilisation site is of crucial importance in both the release profile of the drug in the target locus and its bio-availability.

In the present work the use of a model drug instead of a drug has been preferred for several reasons. We have chosen a peculiar and versatile probe, the Nile Red (NR), because it presents several advantages: (1) it possesses intermediate lipophilicity ($\log P \approx 3-5$) similar to that of the potent chemotherapy drug, such as Paclitaxel; (2) its peculiar spectroscopic behaviour is very sensitive to the medium environment; (3) it is pH insensitive; (4) it is very cheap with respect to active pharmaceutical drugs; (5) it is sequentially metabolised by cytochrome P4503A4 to the N-monoethyl and N-desethyl products, which typifies the metabolism of many amine-containing drugs.

The results for simple model systems represent a first step towards understanding the action and biological properties of anticancer drugs and help to elucidate the behaviour of the drug *in vitro and* subsequently *in vivo*. With this way of proceeding, it is possible to gather useful information before properly optimising the final device based on clay to be used for the modified delivery of the drug.

Experimental part

Materials

The reactants polyoxyethylene sorbitan monolaurate (Tween 20, TW20), Nile Red (NR), hydrochloric acid (HCl), sodium hydroxide standard (NaOH) solutions, acetone were purchased from Sigma–Aldrich and used without any further purification.

Stock solutions of all chemicals used were prepared by weight before use. Deionised water from reverse osmosis (Elga, model option 3), having resistivity higher than 1 MΩ cm, was used to prepare all solutions.

Sample preparation

Aqueous HCl or NaOH solutions at the desired pH were prepared by proper dilution of the corresponding standard solution.

Tween 20 aqueous stock solutions were prepared by weighting the surfactant and solubilising it with the aqueous solution at the required pH, when necessary the pH was adjusted by adding small aliquots of concentrated aqueous HCl or NaOH solutions. Proper dilutions with the aqueous solution at the desired pH have been made to vary the surfactant concentration in the range $1.0 \cdot 10^{-6}$–$1.5 \cdot 10^{-2}$ mol dm^{-3}.

The NR aqueous solutions have been prepared accordingly to the procedure described elsewhere [6]: briefly, the NR-loaded aqueous micelles have been prepared by weighting the model drug and solubilising it acetone, and, then, adding the proper aliquot of this solution, to obtain a NR final concentration of $8.0 \cdot 10^{-6}$ - mol dm^{-3}, to the series of TW20 aqueous solutions prepared as above described.

Surface tension measurements

The surface tension (γ) of aqueous solutions of TW20 (blank micelles) has been measured as a function of the surfactant concentration and at different pH by using a KSV-Sigma 70 automatic tensiometer by applying the Wilhelmy plate method. All the experiments have been performed at room temperature stirring each solution for 60 s and, then, equilibrating it for other 60 s.

Spectrophotometric measurements

The UV−vis spectra of either the blank micelles or the NR loaded-micelles were monitored with a computer controlled Analytic Jena S600 diode array spectrophotometer equipped with compartments for 1 × 1 × 5 cm quartz cells and a magnetic stirring apparatus. The spectra have been registered for 8 h every 15 min on varying both the pH and surfactant concentration. The temperature control was obtained by a thermostat Heto Therm (Thermo Karlsruhe, Germany) $t \pm 0.1$ °C. As previously obtained for other systems [7], the experiments were reproducible only when the samples were not placed in the first position of the spectrophotometer. This has been attributed to the time of exposure to the UV radiation during the course of the experiment, which in turn depends on the position of the cuvettes within the spectrophotometer. In particular, we have to take into account that the first position of the instrument is continuously subjected to the UV radiation, while in the other ones the samples are irradiated only for the time required for the measurements.

Triplicate experiments were performed and the surfactant concentrations were kept the same in the reference and measurement cells to eliminate the effect on UV absorbance of all components the aqueous solution except the NR.

To estimate the NR binding constants the spectrophotometric measurements have been gathered at 25.0 °C, by keeping constant the NR concentration at $8.0 \cdot 10^{-6}$ mol dm^{-3}, over a wide pH range from 1.0 to 7.4 on varying surfactant concentration from 0 to 0.01 mol dm^{-3}.

Deconvolution of the NR-loaded micelles UV–vis spectra

The band shape of the NR-loaded micelles aqueous solutions, under the different experimental conditions applied, was not symmetric, more precisely it is not composed by a single band; thus the deconvolution method has been used to resolve the sub-bands buried in the spectrum, where the sum of the optimum number of sub-bands was required to perfectly match the original contour of the spectrum. UV–vis spectra have been resolved into three/four gaussian components by means of an home-made Matlab ® procedure performing a two-step iterative lest-squares nonlinear fitting of the experimental data, preliminarily smoothed by a moving average technique to reduce or eliminate short-term fluctuations in the data. The first fitting procedure interpolates a linear baseline from the edges of the data segment and subtracts it from the signal.

The optimisation algorithm adopted in the preliminary step uses the Nelder–Mead simplex method as previously described [8]. This algorithm uses a simplex of $n + 1$ points for n-dimensional vectors **x**.

For each run a multiple trial fit with different guess values has been made, choosing as starting point those yielding the lowest mean absolute error on the fit. Once the spectrum have been resolved, the peaks parameters have been used as starting values in a nonlinear least-squares regression, in order to improve the estimates still further and to apply the regression diagnostics. Because of the low noise of the spectroscopic data, no robust fitting has been used, which would be effective in other situations with much more noised spectra.

It has been obtained that the best results have been reached when refining fixed-width Gaussian functions, as sometimes adopted in spectroscopic analyses.

Results and discussion

Surface tension data

The air/solution interfacial behaviour of the TW20 at different pH has been monitored on increasing surfactant concentration. In addition, the surface tension of the aqueous solution at the highest surfactant concentration was measured after 4 days (by storing the samples in the dark) from preparation and, it has been found that it remains almost unchanged with respect to that of the freshly prepared solution. This result evidences that, under the different experimental conditions applied, the Tween 20 aqueous solutions are stable over time.

For all cases studied, the decrease in γ on increasing polysorbate concentration is normally sigmoid or near sigmoid in nature, thus indicating that the bio-compatible surfactant acts in the classical way, i.e., at low surfactant concentration, the surface tension of aqueous solutions of surfactants decreases with addition of surfactant until the cmc is reached and, then, remains almost constant above the critical value. Nevertheless, in our cases, the registered γ values do not attain a plateau but monotonically decrease on augmenting the [TW20] and also a neat break, as expected, was not obtained. These results might be reasonably attributed to the composition of the Tween 20 surfactant. In fact, the wide distribution in the ethoxylation may suggest to consider the polysorbate as a mixture of surfactant, thus, its behaviour at the air/solution interface is similar to that of mixed surfactant [9].

The critical micelle concentrations of polysorbate 20 in aqueous solution at different pH have been estimated as the intersection point of the two linear plots, above and below the cmc, of the surface tension vs. log [Tween 20].

The obtained cmc_s values as a function of the pH are collected in Table 1.

The order of magnitude of the cmc_s values obtained in the present work is in good agreement with that reported in the literature [10–13] however, a direct comparison is difficult because different

Table 1
cmc_s values of TW20 aqueous solutions a function of pH at $T = 25.0$ °C.

pH	cmc (10^{-5} mol dm^{-3})
1.0	3.58
1.8	1.65
2.5	0.92
5.5	0.84
7.4	0.49

lots of commercially available samples of Tween 20 were used and, above all, the different experimental conditions used in the present work cannot be leaved out of consideration.

It can be noticed that the aggregation process takes place at very low surfactant concentration whose value depends to a certain extend on the pH and on the type of electrolytes used for keeping constant the pH, namely HCl or NaOH. In particular, increasing the amount of HCl in the aqueous medium, i.e., from pH 5.5 to 1.0, leads to an enhancement of the cmc values while replacing the chloride ion with the hydroxide, to keep the pH at 7.4, brings about the opposite effect. The observed cmc vs. pH profile, can be explained by considering that, at low pH both the H^+ and the Cl^- contrast the hydrophobic interactions. In fact, protonation of the oxygen of the ether groups makes the surfactant head groups cationic, thus electrostatic repulsion among the head groups unfavoured the micelle formation, simultaneously the chloride ions exert their structure-breakers action. This way, since the micelle formation of nonionic surfactants is mainly governed by hydrophobic interactions [14] both ionic species by lowering the hydrophobic effect to a certain extent modestly enhances the cmc values. A similar cmc trend has been previously [15] obtained for the micellization process of the TW20 in the aqueous solution containing increasing amount of another structure-breakers solute, namely ethyleneglycol. As for the micellization process at physiological pH conditions, presence of hydroxide ions which act as structure-makers by exalting the hydrophobic effect induces the self-organisation of the polysorbate biosurfactant at very low concentration. Moreover, analogues pH trends have been reported for the Tween 40 aqueous solutions [16].

Since the pH is of considerable pharmaceutical relevance for both the drug loading and releasing behaviour, we can reasonably propose that the delicate balance between hydrophilic and hydrophobic interactions lead to the formation of aggregated systems whose specific hosting capability can be easily tuned by changing the crucial pH parameter.

Spectrophotometric data

The stability of both the blank and NR-loaded TW20 nonionic surfactant aqueous solutions, under the experimental conditions used in the present work, has been ascertained by monitoring the UV–vis spectra of the aqueous solutions as a function of both the surfactant concentration and time. For each solution, as the overlapping processes for each spectrum show, no noteworthy changes neither in the intensity nor in the position of the band has been detected in the timeframe of observation, indeed the band shape does not modify. This way, we could draw the conclusion that every surfactant aqueous solution does not undergo any chemical modification with the time and presence of NR does not reciprocally alter the components stability. Moreover, at the highest surfactant concentration, the registered spectra after 4 days (by storing the samples in the dark) from preparation resulted to completely match with the previous one, further corroborating the aqueous solution stability assessed by means of the complementary tensiometric measurements.

As concerns the form, the position and the intensity of the band on varying the bio-surfactant concentration the overlapping process of all spectra evidences that all of these spectral characteristics strongly depend on the surfactant concentration and the applied pH plays a relevant role. Typical spectra are shown in Fig. 1. For all cases examined, the NR-loaded micelles spectra at TW20 concentration below the cmc are slightly affected by the presence of surfactant, thus indicating no significant interaction between the model drug and the free Tween 20 molecules. The surfactant concentration values at which detectable change in the spectral parameters have been evidenced was slightly higher than the cmc tensiometrically determinate. This result might be ascribed to the shift of the micellization process due to the presence of an hydrophobic molecules [4,10]. Therefore, the cmc values determined from the change in the absorption spectrum of NR aqueous solution have been considered in the calculations.

It has been found that, for TW20 concentration above the cmc, a progressive blue-shift in the principal maximum position occurs until an invariance of the position is achieved due to the micelle formation. These results suggested that, on increasing surfactant concentration the NR model drug experiences a more and more hydrophobic medium, which remains the same once the aggregated system is formed. Moreover, for all the experimental conditions applied, the shape of the band is not symmetric. This could imply that either the hydrophobic model drug can aggregate forming the dimeric species (or even higher aggregates) or the NR experiences diverse zones of polarity which bring about different contributes to the total absorbance. The choice between these two possibilities has been done by considering that the asymmetry endures even at the highest [TW20]. Since high surfactant concentrations reduces the drug aggregation process we have reasonably assumed that the NR is confined in specific solubisation sites, whose contribution to the spectra shape depends on the applied experimental conditions, namely pH and surfactant concentration. As a result of these considerations, the analysis of the spectrophotometric data has been performed by means of the deconvolution method (see Experimental section for the details). This proper and precise procedure allow to resolve the sub-bands buried in the spectrum and from the dependence of the specific intensity on the surfactant concentration, at each λ_{max}, allow the estimation of the affinity of the NR for the different solubilisation *loci*. Comparison with the conventional method, which provides only one binding constant value at the wavelength of the maximum intensity, has also done by applying the two pseudo-phases model.

Spectrophotometric data treatment by the non-conventional pseudo-phases model

Typical deconvoluted UV–vis spectra have been shown in Fig. 2.

As already stated both the variations of the TW20 concentration and the medium pH play a relevant role in influencing the spectroscopic behaviour of the NR-loaded TW20 aqueous solutions. For each studied situation, the deconvolution analysis provided information on the band positions and intensities. In particular, four sub-bands, whose intensities vary on [TW20] augmentation, have

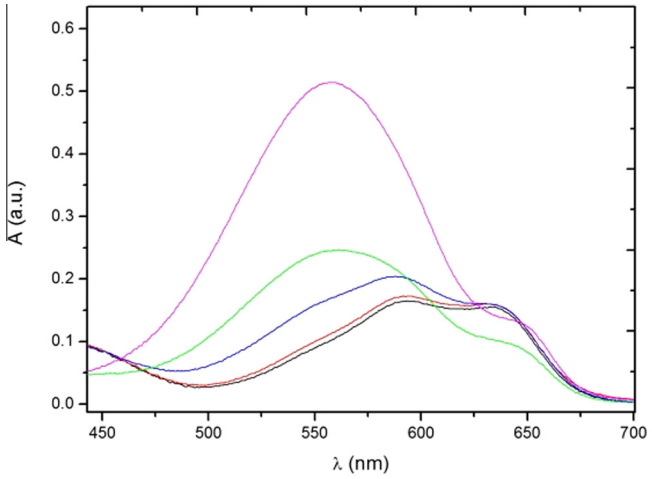

Fig. 1. Tipical UV–vis spectra of $8.0 \cdot 10^{-6}$ mol dm^{-3} NR aqueous surfactant solution at pH = 1.0 as a function of TW20 concentration. (–) [TW20] = 0 mol dm^{-3}, (–) [TW20] = $2.0 \cdot 10^{-6}$ mol dm^{-3}, (–) [TW20] = $3.0 \cdot 10^{-4}$ mol dm^{-3}, (–) [TW20] = $2.0 \cdot 10^{-3}$ mol dm^{-3}, (–) [TW20] = $1.0 \cdot 10^{-2}$ mol dm^{-3}. T = 25.0 °C.

been found at very low pH values, i.e., 1.0 and 1.8, and this number reduces to three on increasing pH.

The obtained maximum wavelengths of each peak in the post micellar region are 630, 570, 530 and 490 nm for the extremely acidic conditions and 570, 530 and 490 nm for the other pH values. The band position can be reasonably associated, from the higher to the lower wavelength accordingly to the decreasing environment polarity, to the NR confined in the aqueous solution and in the three micellar solubisation sites, namely polar head group, palisate layer and micellar core. An analogous procedure for the attribution of the band position has been reported by several researchers by analysing the fluorescents findings [17–19].

It has to be highlighted that the peak intensities are enhanced by the presence of the polysorbate with exception of that at 630 nm which vanishes on increasing both the TW20 concentration and the medium pH. The explanation of these apparently unusual results relies on the interplay of the hydrophilic and/or hydrophobic interactions involved between the model drug and the specific micellar solubilisation *locus*, strictly depend on the medium pH, i.e., the palisade layer. In particular, at very low pH the hydrophobic NR might add a proton at the cyclic nitrogen atoms [20,21] and/or form molecular aggregates. In both cases, the less hydrophobic species confined in the aqueous pseudo-phase justify the presence of the red band that disappears because either the positive charge are shielded by increasing the pH or there is an higher number of micelles able to host the NR, thus, hampering the drug aggregation. Moreover, the capability of NR to form protonated species has also been proposed for the interactions of the sparingly water soluble probe with the cyclodextrins [22].

It has been obtained that, in all cases studied, the absorbance value increases with increasing polysorbate concentration until it reaches a plateau value. Nevertheless, in the light of the deconvolution results we cannot consider that the drug partition occurs between the micellar pseudo phase and water but binding of the NR to the three specific solubilisation sites has to be taken into account. Thus, we have extended the two pseudo-phases model [23] accordingly to the following equilibria:

$$NR_W \rightleftarrows NR_{HG} \quad (1)$$

$$NR_W \rightleftarrows NR_P \quad (2)$$

$$NR_W \rightleftarrows NR_C \quad (3)$$

with a binding constant $K_{\beta/W}$, where β represents the different pseudo-phase, given by:

$$K_{HG/W} = \frac{[NR]_{HG}}{[NR]_W \cdot C} \quad (4)$$

$$K_{P/W} = \frac{[NR]_P}{[NR]_W \cdot C} \quad (5)$$

$$K_{C/W} = \frac{[NR]_C}{[NR]_W \cdot C} \quad (6)$$

where C = [TW20] − cmc represent the micellized surfactant.

This way, at each pH and λ_{max}, the absorbance of the aqueous solution results from the contribution of the NR confined in the specific pseudo-phases. The specific absorbance profile as function of C is given as:

$$A_{HG/W} = A_W + \frac{(A_{HG} - A_W)K_{HG-W}C}{1 + K_{HG-W}C} \quad (7)$$

$$A_{P/W} = A_W + \frac{(A_P - A_W)K_{P-W}C}{1 + K_{P-W}C} \quad (8)$$

$$A_{C/W} = A_W + \frac{(A_C - A_W)K_{C-W}C}{1 + K_{C-W}C} \quad (9)$$

where A_W, A_{HG}, A_P and A_C represent the absorbance of the NR in the different pseudo-phases for each λ_{max}, namely water, polar head groups, palisade layer and core, respectively.

Robust nonlinear least-squares fitting of the spectrophotometric data allows for an estimation of the binding constant values of the NR to the specific polarity solubilisation *locus*.

Robust treatment of the spectrophotometric deconvoluted data

The binding constant values ($K_{\beta/W}$) have been estimated by fitting the intensities of each band accordingly to Eqs. (7) and (9),

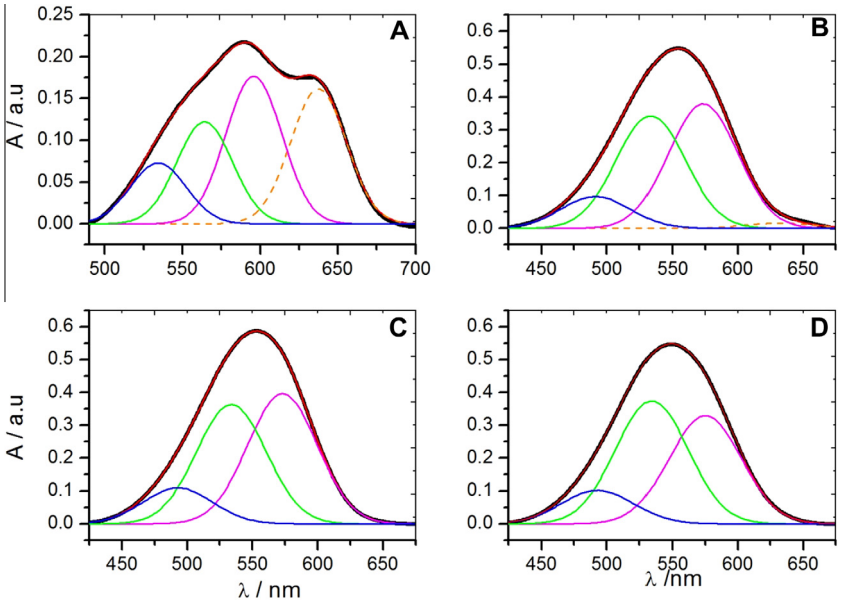

Fig. 2. Typical UV–vis deconvoluted spectra of $8.0 \cdot 10^{-6}$ mol dm^{-3} NR aqueous surfactant on varying both pH and TW20 concentration at $T = 25.0$ °C. (A) pH = 1.0 [TW20] = $3.0 \cdot 10^{-4}$ mol dm^{-3}, (B) pH = 1.9 [TW20] = $8.0 \cdot 10^{-3}$ mol dm^{-3}, (C) pH = 2.5 [TW20] = $8.0 \cdot 10^{-3}$ mol dm^{-3}, (D) pH = 7.4 [TW20] = $9.1 \cdot 10^{-4}$ mol dm^{-3}. (▬) experimental and (–) calculated curve profile.

Table 2
Selected figures of merit for the λ_{max} = 530 nm – pH 1.0 case regressions with the whole data set and after the elimination of one outlier. Acronyms explanation and related definitions are in appendix A.

	Whole data set	Outlier elimination
$(n-p)$	17	16
ANOVA		
SSM	0.12965	0.12715
SSR	0.00233	0.00121
SST	0.13198	0.12836
F calc.	473.24	841.64
MSSE	0.00014	0.00008
RMSSE	0.01170	0.00869
R	0.99114	0.99528
R^2	0.98236	0.99058
R^2_{adj}	0.98028	0.98941
Parameters statistics		
A_W	0.079902	0.073408
A_P	0.356815	0.357019
$K_{P/W}$	860.2166	887.0112
s.u. (A_W)	0.008237	0.006408
s.u. (A_P)	0.009073	0.006611
s.u. ($K_{P/W}$)	129.6513	96.5269
t calc. (A_W)	9.70	11.46
t calc. (A_P)	39.33	54.00
t calc. ($K_{P/W}$)	6.63	9.19
Non-weighted residuals statistics		
ME	$8.47 \cdot 10^{-8}$	$1.01 \cdot 10^{-7}$
σ	0.011071	0.008194
Jarque–Bera statistic for normality of residual		
JB	3.66	0.16
χ^2_{crit} (0.01)	9.21	9.21
Passed prob.	0.16	0.92
Shapiro–Wilk statistic for normality of residuals		
W	0.94	0.98
W_{crit} (0.01)	0.87	0.86
Passed prob.	0.31	0.93
Modified Levene test for constant variance		
MLT	1.51	0.06
MLT_{crit} (0.01)	8.28	8.40
Passed prob.	0.24	0.92
Model comparison		
PRESS	0.00326	0.00211
MEP	0.00016	0.00011
R^2_{pred}	0.97533	0.98355
AICc	−173.663	−175.992

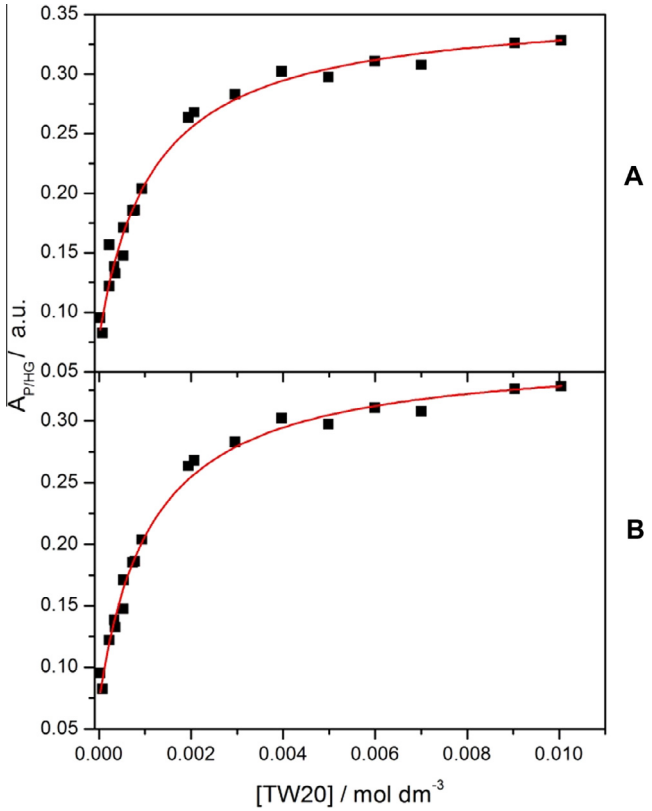

Fig. 4. Typical absorbance profiles of $8.0 \cdot 10^{-6}$ mol dm^{-3} NR, at the λ_{max} = 530 nm pH = 1.0, on varying the TW20 concentration and T = 25.0 °C. (A) Case with the whole data set, (B) after the elimination of one outliers (i.e., the observation ($2.3 \cdot 10^{-4}$, 0.1566). (■) experimental data and (–) curve calculated by a non-linear least square fit to Eq. (9).

using a robust nonlinear least-squares method implemented in the Solverstat [24] Excel ® macro. Because of the natural noise affecting this kind of data an iteratively reweighted least-squares regression using the Huber robust weight function has been adopted [25]. For each run, moreover, a (robust) regression diagnostic to detect the possible outlier has been applied. This check has been particularly

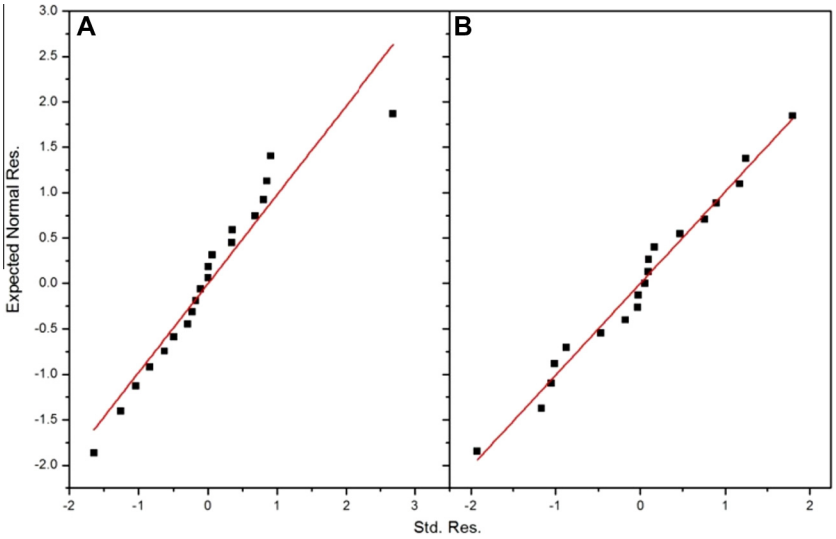

Fig. 3. Expected normal standard residuals vs. Observed standard residuals for the λ_{max} = 530 nm – pH 1.0 (A) case with the whole data set, (B) case after the elimination of one outlier. (■) experimental data and (–) theoretical values.

effective in eliminating the inevitable aberrant data points that in such a kind of systems would dramatically noise the estimates (especially the evaluation of $K_{\beta/W}$). Thus, a comparison of the leverage, Cook's distance, studentised residual and COVRATIO values has been performed (see Appendix A for a complete list of the acronyms and explanation here adopted) in order to detect and eliminate the actual outlier of the refinement, following a procedure as described in the literature [26]. The data points with all of the values exceeding the commonly adopted thresholds for the above listed statistics [27] have been eliminated from the data set, yielding a significant reduction of the noise on the estimates. As an example of the effectiveness of this procedure, we have reported here the λ = 530 nm – pH 1.0 case, which represents a situation with just one outlier. Such a case would give a general sense of how a regression is likely to be biased even by the presence of just one aberrant observation. The number of observations in the whole data set was 20, but the regression diagnostics showed the presence of a dangerous outlier represented by the point at ($2.27 \cdot 10^{-4}$, 0.1566). This observation has COVRATIO = 0.18 (extremely less than the threshold $1 - 3p/n = 0.52$), and stud. Del. residual = 3.9 (greater than the threshold = 3). After the elimination of this outlier, which the robust procedure is still not able to successfully underweight, the regression results much more improved, as can be evaluated by perusal of Table 2, in which a number of selected figures of merits and statistical diagnostics are reported. A pictorial representation of the effectiveness of the outlier elimination is depicted in Fig. 3 (where a comparison of the expected/observed std. residuals before and after the elimination is plotted respectively), while in Fig. 4 the observed/calculated patterns for the whole data set case and the purged one are plotted respectively.

A comparison of the classic diagnostics represented by R, R^2 and R^2_{adj} as well as the s.u.'s associated to each variable suggests that the outlier elimination has actually improved the estimation.

The determination coefficient R^2 was 0.982 with the whole data set and 0.991 after the outlier elimination; the s.u.'s associated to each parameter have fallen by 20–27%. Further corroboration of this behaviour is represented by some test on the regression such as the Jarque–Bera Statistic for Normality of Residual, whose probability to reject the associated null hypothesis increases from 20% to 90%, as well as the modified Levene test for constant variance, whose associated probability of success increases from 25% to 90%. The most important tests to choose in a rigorous way the model are represented by the model comparison statistics, such as PRESS statistics (i.e., the predicted residual for the each case that results from omitting the case itself from estimation), which lowers by ≈35%, MEP (i.e., cross-validation mean error of prediction, which gives a rough description of the performance of the model), improved by ≈30%, and, overall, by the Akaike Information Criterion (AIC). This statistics belongs to the family of the Bayesian Information Criteria for the model comparison: the model having the lowest AIC value is the best one (in our case the model with outlier elimination).

Also the R^2_{pred} value, which gives an idea of the prediction capability of the model, results improved passing from 0.975 to 0.984 after eliminating the aberrant observation. It is straightforward that the improvement of the estimates turns into a very significant improvement of the subsequent evaluations that are function of the estimated parameters, especially for what concerning the $K_{\beta/\alpha}$ values (Table 3).

For the sake of accessibility the $K_{\beta/W}$ have been extracted from the above reported table and are shown in Table 4.

Inspection of the Table 4 reveals that the confining ability of the different polarity zones of the micelle towards the NR binding is strongly favoured by the increase in the pH and the palisade layer is the region that is much more affected by this parameter. In fact, the pH augmentation leads to an increase of the specific binding capacities of a factor ca. 14, 42 and 5, to the HG, P and C pseudophase, respectively.

Table 3
Refined parameters and selected figures of merits (f.o.m.) for the non-linear regressions according to Eqs. (7) and (9). prob. = probability to reject the null hypothesis for the related statistical test.

	pH				
	1.0	1.8	2.5	5.5	7.4
λ = 570 nm refined parameters					
A_W	0.1557	0.2641	0.2389	0.1203	0.1313
A_{HG}	0.2527	0.4062	0.4088	0.3991	0.3542
$K_{HG/W}$	316.56	751.08	1452.14	3142.86	4523.71
s.u. (A_W)	0.0042	0.0192	0.0063	0.0211	0.0101
s.u. (A_{HG})	0.0081	0.0065	0.0042	0.0043	0.0072
s.u. ($K_{HG/W}$)	39.63	296.82	223.61	530.96	851.45
Regression f.o.m.					
RSS	$8.75 \cdot 10^{-4}$	$9.01 \cdot 10^{-5}$	$4.49 \cdot 10^{-5}$	$1.89 \cdot 10^{-3}$	$1.47 \cdot 10^{-3}$
MSE	$4.17 \cdot 10^{-5}$	$1.29 \cdot 10^{-5}$	$7.48 \cdot 10^{-6}$	$8.58 \cdot 10^{-5}$	$1.22 \cdot 10^{-4}$
R^2	0.9904	0.9866	0.9969	0.9748	0.9783
R^2_{adj}	0.9894	0.9799	0.9949	0.9721	0.9735
R^2_{pred}	0.9864	0.9341	0.9730	0.9675	0.9423
JB (prob.)	0.68	0.20	0.43	0.59	0.59
	(0.71)	(0.91)	(0.81)	(0.75)	(0.74)
MLT	0.08	0.51	0.01	0.01	0.66
(prob.)	(0.77)	(0.51)	(0.99)	(0.99)	(0.54)
λ = 530 nm refined parameters					
A_{HG}	0.0734	0.0068	0.2480	0.1633	0.1283
A_P	0.3570	0.3546	0.3700	0.3746	0.3402
$K_{P/HG}$	887.01	7880.79	13368.79	28517.27	37558.24
s.u. (A_{HG})	0.0064	0.0904	0.0535	0.0139	0.0100
s.u. (A_P)	0.0066	0.0019	0.0029	0.0009	0.0040
s.u. ($K_{P/HG}$)	96.53	2841.31	9730.16	3962.47	6787.90
Regression f.o.m.					
RSS	$1.21 \cdot 10^{-3}$	$2.74 \cdot 10^{-5}$	$6.39 \cdot 10^{-5}$	$5.72 \cdot 10^{-6}$	$7.81 \cdot 10^{-4}$
MSE	$7.55 \cdot 10^{-5}$	$3.91 \cdot 10^{-6}$	$7.99 \cdot 10^{-6}$	$8.18 \cdot 10^{-7}$	$9.76 \cdot 10^{-5}$
R^2	0.9906	0.9965	0.9762	0.9994	0.9822
R^2_{adj}	0.9894	0.9948	0.9603	0.9990	0.9777
R^2_{pred}	0.9894	0.9401	0.9588	0.9244	0.9796
JB (prob.)	0.16	0.44	0.21	0.33	0.83
	(0.92)	(0.80)	(0.90)	(0.85)	(0.85)
MLT	0.06	0.60	0.64	0.05	0.05
(prob.)	(0.92)	(0.60)	(0.72)	(0.84)	(0.84)
λ = 490 nm refined parameters					
A_P	0.0509	0.0332	0.0384	0.0367	0.0001
A_C	0.1209	0.0994	0.1140	0.1164	0.1212
$K_{C/P}$	1648.71	2685.76	3110.26	5678.71	7231.17
s.u. (A_P)	0.0010	0.0068	0.0070	0.0091	0.0088
s.u. (A_C)	0.0009	0.0015	0.0026	0.0018	0.0016
s.u. ($K_{C/P}$)	101.33	978.21	827.58	1488.05	1268.15
Regression f.o.m.					
RSS	$3.07 \cdot 10^{-6}$	$1.35 \cdot 10^{-5}$	$1.11 \cdot 10^{-4}$	$2.76 \cdot 10^{-4}$	$9.97 \cdot 10^{-6}$
MSE	$3.07 \cdot 10^{-7}$	$1.50 \cdot 10^{-6}$	$1.01 \cdot 10^{-5}$	$1.32 \cdot 10^{-5}$	$9.06 \cdot 10^{-7}$
R^2	0.9980	0.9947	0.9699	0.9503	0.9977
R^2_{adj}	0.9975	0.9911	0.9623	0.9447	0.9962
R^2_{pred}	0.9311	0.9211	0.8986	0.8801	0.8674
JB (prob.)	0.87	0.47	0.44	0.20	0.57
	(0.64)	(0.79)	(0.81)	(0.90)	(0.75)
MLT	0.31	0.29	0.76	0.98	1.08
(prob.)	(0.58)	(0.61)	(0.50)	(0.40)	(0.34)

Table 4
Binding constants ($K_{\beta/W}$) values of NR confined in the three specific solubilisation sites of TW20 micelles.

pH	10^{-3} $K_{HG/W}$ (dm^{-3} mol^{-1})	10^{-3} $K_{P/HG}$ (dm^{-3} mol^{-1})	10^{-3} $K_{C/P}$ (dm^{-3} mol^{-1})
1.0	0.32 ± 0.04	0.9 ± 0.1	1.6 ± 0.9
1.8	0.8 ± 0.3	8 ± 2	2.7 ± 0.6
2.5	1.5 ± 0.2	13 ± 9	3.1 ± 0.9
5.5	3.1 ± 0.5	30 ± 10	6 ± 1
7.4	4.5 ± 0.8	38 ± 6	7 ± 2

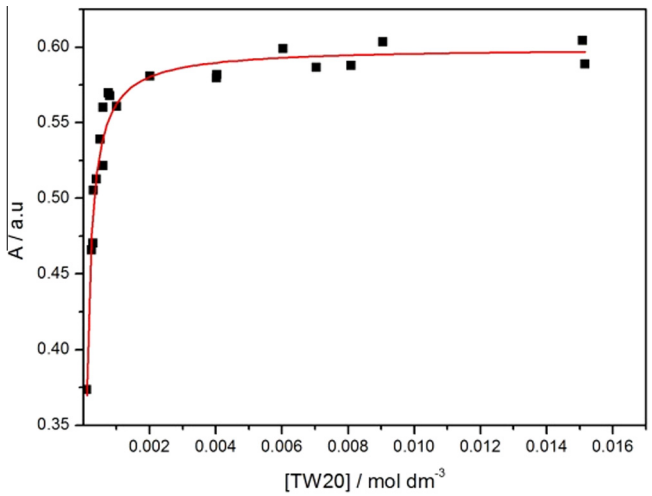

Fig. 5. Typical absorbance profiles of $8.0 \cdot 10^{-6}$ mol dm^{-3} NR as a function of the TW20 concentration at pH = 5.5, λ_{max} = 553 nm and T = 25.0 °C. (■) experimental data and (–) curve calculated by applying the equation of two pseudo-phases model.

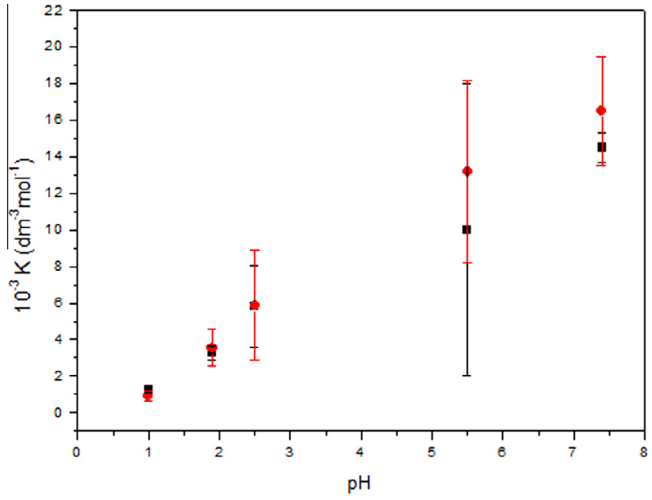

Fig. 6. Binding constants of NR in TW20 calculated with the two pseudo-phases model (■), and by averaging the values of the binding constants of NR (Table 4) in the three specific solubilisation sites of TW20 micelles (●).

The obtained binding trends are in good agreement with the surface tension results and allow to draw the conclusion that the simultaneous and progressive depletion of both the positive charge present in the polyoxyethylene head groups and the presence of the structure-breaker/maker anions favour the formation of different aggregated systems, whose hydrophilic/hydrophobic nature depend to a diverse extent on the pH. Anyway, in all cases, the pH change exalts the hosting capability towards the sparingly water soluble NR. However, the palisade layer is the region that much more is affected by the destruction of the pH-dependent structure, which in turn, provides a peculiar environment that optimise the hydrophilic and/or hydrophobic interactions.

Spectrophotometric data treatment by classical two pseudo-phases model

As for the dependence of the maximum intensity on the surfactant concentration, for all cases studied, a typical example is depicted in Fig. 5.

It has been noticed that the maximum wavelength does not coincides with any of the values obtained with the deconvolution procedure but it is an intermediate value between the polar head group and the palisade layer wavelengths (557–552 nm depending of the pH). Nevertheless, the intensity trends as a function of both pH and surfactant concentration are similar of those above reported. The robust data treatment by applying the two pseudo-phases model, which we recall, assumes the aqueous aggregated system as a pseudo-phase separated from the aqueous one, yields different binding constant values. The binding constant values are collected in Fig. 6.

Comparison of the local and the overall binding values K evidences that the former seems to represent an intermediate situation between the three local bindings, thus, suggesting to calculate, at each pH, the mean value $\langle K \rangle$ by means of $K_{HG/W}$, $K_{P/W}$, $K_{C/W}$. As it can be noticed from the data listed in Fig. 6 the averaged binding values $\langle K \rangle$ are in good agreement with those calculated with the two pseudo-phases model. This result clearly suggests that the deconvolution procedure provides more precise and reliable values, which, above all, are much more representative of the drug confinement.

Conclusions

The information gathered in the present work allow to draw the conclusion that the deconvolution procedure by applying an extended classical two pseudo-phases-model provides more precise and reliable values of the NR binding constants to the specific polarity solubilisation *loci* of TW20 micelles with respect to the classical data treatment, which only provides an averaged hosting capability of the micellar aggregate. The confining ability of the TW20 aggregated systems can be easily tuned by changing the pH, which reflects, first of all the delicate interplay between hydrophilic and hydrophobic interactions, then, evidences that the confinement of the model drug in the different solubilisation sites makes the TW20 aggregates systems as a good candidate to be used for the organophobic transformation of the clay, consequently for the modified drug delivery. Moreover, it can be reasonably suggested that the diverse partition of the drug into the pseudo-phases would strongly influences not only the drug release profiles but also the bioavailability and the action in the suitable action site.

Acknowledgements

The authors gratefully acknowledge the financial support provided by the Italian Ministry of the Research (MIUR) (PRIN Grant 2010EARRRZ_003) and local founds from University of Palermo (ex 60%). The authors also tanks Mr. Pietro Bisconti (University of Palermo) for experimental help.

Appendix A. Notes

n = number of observations.

p = number of parameters.

SSM = model sum of squares, i.e., the sum of the squares of the differences between the predicted values and the mean value of the response variable.

SSR = residuals sum of squares, i.e., the sum of the squares of the discrepancies between the observed and the calculated data points.

SST = total sum of squares, i.e., the sum of the squares of the difference between each dependent variable and its mean.

F calc. = F statistic test, i.e., the test that all the regression coefficients are zero. In models comparison, the higher is the F calc. value the better is the model.

MSSE = error mean sum of squared, i.e., a measure of the measures the average of the squares of the errors. High values are due to randomness or inaccuracy of the estimator.

RMSSE = root of MSSE.

R = correlation coefficient.

R^2 = coefficient of determination, as commonly defined as $1 - \mathrm{SSR/SST}$.

R^2_{adj} = adjusted R^2, defined as $1 - (\mathrm{SSR/dfr})/(\mathrm{SST/dft})$, where dft is the degrees of freedom $n - 1$ of the estimate of the population variance of the dependent variable, and dfr is the degrees of freedom $n - p - 1$ of the estimate of the underlying population error variance. When comparing models, it takes into account the effects due to extra explanatory variables added to the model.

s.u.(x) = Standard Uncertainty associated to the parameter x.

t calc.(x) = t-statistic value for the parameter x.

PRESS Del. residuals = the predicted residual for the each case that results from omitting the case itself from estimation.

COVRATIO = measure of the effect of observations on the covariance matrix of the parameter estimates. Values of COVRATIO near 1 indicate that the observation has little effect on the precision of the estimates. Observations with $|\mathrm{COVRATIO} - 1| > 3p/n$ suggest a need for further investigation; in particular, $\mathrm{COVRATIO} < 1 - 3p/n$ identifies a dangerous outlier to be eliminated.

ME = mean error of the residuals.

σ = standard deviation of the residuals.

JB = Jarque–Bera statistic for normality of residual; it must be $< \chi^2_{crit}$. It is a goodness-of-fit test of whether sample data have the skewness and kurtosis matching a normal distribution. $\chi^2_{crit}(0.01)$ = critical value of the χ^2 distribution at $\alpha = 0.01$.

W = Shapiro–Wilk statistics for the normality of residuals; it must be $< W_{crit}$.

MLT = modified Levene test; it must be $< MLT_{crit}$.

Passed prob. = the probability that the null hypothesis of the related statistical test is false.

PRESS = cross-validation model giving a measure of the fit of a model to a sample of observations that were not themselves used to estimate the model. It is calculated as the sums of squares of the above defined PRESS Del. residuals.

MEP = cross-validation mean error of prediction, which gives a rough description of the performance of the model, and it depends on the unknown response function and the unknown variance of the observations. Best models have lower MEP.

R^2_{pred} = prediction R^2, defined as $1 - \mathrm{PRESS/SST}$.

AICc = corrected Akaike Information Criterion, i.e., a measure of the relative quality of a statistical model, for a given set of data and regressors. As such, AICc provides a means for model selection (best model = min AICc).

References

[1] I. Calabrese, G. Cavallaro, C. Scialabba, M. Licciardi, M. Merli, L. Sciascia, et al., Montmorillonite nanodevices for the colon metronidazole delivery, Int. J. Pharm. 457 (2013) 224–236, http://dx.doi.org/10.1016/j.ijpharm.2013.09.017.

[2] B.A. Kerwin, Polysorbates 20 and 80 used in the formulation of protein biotherapeutics: structure and degradation pathways, J. Pharm. Sci. 97 (2008) 2924–2935, http://dx.doi.org/10.1002/jps.21190.

[3] M. Yang, F. Cui, B. You, J. You, L. Wang, L. Zhang, et al., A novel pH-dependent gradient-release delivery system for nitrendipine. I. Manufacturing, evaluation in vitro and bioavailability in healthy dogs, J. Controlled Release 98 (2004) 219–229, http://dx.doi.org/10.1016/j.jconrel.2004.04.022.

[4] M. Enache, E. Volanschi, Spectroscopic investigations of the molecular interaction of anticancer drug mitoxantrone with non-ionic surfactant micelles, J. Pharm. Pharmacol. 64 (2012) 688–696, http://dx.doi.org/10.1111/j.2042-7158.2012.01445.x.

[5] S.C.M. Marcus, J.B. Hauser, The solubilization site of 5,10,15,20-tetrakis-(2,6-dichlorophenyl)-porphyrin-Mn(III) in DPPC vesicles: a spectrophotometric and tensiometric study, Colloids Surf. Physicochem. Eng. Asp. 278 (2006) 212–217, http://dx.doi.org/10.1016/j.colsurfa.2005.12.019.

[6] S. Hassoon, I. Schechter, A sensitive fluorescence probe for DDT-type pesticides, Anal. Chim. Acta 368 (1998) 77–82, http://dx.doi.org/10.1016/S0003-2670(98)00166-4.

[7] M.L. Turco Liveri, M. Licciardi, L. Sciascia, G. Giammona, G. Cavallaro, Peculiar mechanism of solubilization of a sparingly water soluble drug into polymeric micelles. Kinetic and equilibrium studies, J. Phys. Chem. B 116 (2012) 5037–5046, http://dx.doi.org/10.1021/jp211973s.

[8] J.C. Lagarias, J.A. Reeds, M.H. Wright, P.E. Wright, Convergence properties of the Nelder–Mead simplex method in low dimensions, SIAM J. Optim. 9 (1998) 112–147.

[9] R. Lombardo, C. Sbriziolo, M.L. Turco Liveri, Rate-retarding effects of mixed anionic/non-ionic micelles on the alkaline hydrolysis of the chloropentamminocobalt(III) complex: role of the anionic surfactant chain nature, Colloids Surf. Physicochem. Eng. Asp. 273 (2006) 1–9, http://dx.doi.org/10.1016/j.colsurfa.2005.07.020.

[10] A. Patist, S.S. Bhagwat, K.W. Penfield, P. Aikens, D.O. Shah, On the measurement of critical micelle concentrations of pure and technical-grade nonionic surfactants, J. Surf. Deterg. 3 (2000) 53–58, http://dx.doi.org/10.1007/s11743-000-0113-4.

[11] I. Ullah, M.K. Baloch, G.F. Durrani, Solubility of nonsteroidal anti-inflammatory drugs (NSAIDs) in aqueous solutions of non-ionic surfactants, J. Solution Chem. 40 (2011) 1341–1348, http://dx.doi.org/10.1007/s10953-011-9709-z.

[12] É. Kalmár, K. Ueno, P. Forgó, G. Szakonyi, G. Dombi, Novel sample preparation method for surfactant containing suppositories: effect of micelle formation on drug recovery, J. Pharm. Biomed. Anal. 83 (2013) 149–156, http://dx.doi.org/10.1016/j.jpba.2013.04.039.

[13] M.R.R. Niño, J.M.R. Patino, Surface tension of bovine serum albumin and Tween 20 at the air-aqueous interface, J. Am. Oil Chem. Soc. 75 (1998) 1241–1248, http://dx.doi.org/10.1007/s11746-998-0169-6.

[14] M.J. Schick, Nonionic Surfactants: Physical Chemistry, CRC Press, 1987.

[15] C. Carnero Ruiz, J. Molina-Bolívar, J. Aguiar, G. MacIsaac, S. Moroze, R. Palepu, Effect of ethylene glycol on the thermodynamic and micellar properties of Tween 20, Colloid Polym. Sci. 281 (2003) 531–541, http://dx.doi.org/10.1007/s00396-002-0801-1.

[16] J.R. Bloor, J.C. Morrison, C.T. Rhodes, Effect of pH on the micellar properties of a nonionic surfactant, J. Pharm. Sci. 59 (1970) 387–391, http://dx.doi.org/10.1002/jps.2600590325.

[17] E. Lorente, A. Rodríguez, E. Aicart, E. Junquera, Non-ionic and cationic micelle nanostructures as drug solubilization vehicles: spectrofluorimetric and electrochemical studies, Colloid Polym. Sci. 285 (2007) 1321–1329, http://dx.doi.org/10.1007/s00396-007-1689-6.

[18] G. Hungerford, M. Amaro, P. Martins, M.I. Ferreira, M. Uttamlal, A.S. Holmes-Smith, Effect of polymer strengtheners on the local environment of biocompatible glass as probed by fluorescence, J. Fluoresc. 18 (2008) 297–303, http://dx.doi.org/10.1007/s10895-007-0269-y.

[19] E. Aicart, P. del Burgo, O. Llorca, E. Junquera, Electrochemical, microscopic, and spectroscopic characterization of prevesical nanostructures and vesicles on mixed cationic surfactant systems, Langmuir 22 (2006) 4027–4036, http://dx.doi.org/10.1021/la053474q.

[20] A.Ya. Freidzon, A.A. Safonov, A.A. Bagaturyants, M.V. Alfimov, Solvatofluorochromism and twisted intramolecular charge-transfer state of the Nile Red dye, Int. J. Quantum Chem. 112 (2012) 3059–3067.

[21] N.I. Selivanov, L.G. Samsonova, V.Y. Artyukhov, T.N. Kopylova, Theoretical and experimental investigations of photophysics of the Nile Red molecule and its protonated structures, Russ. Phys. J. 54 (2011) 601–606, http://dx.doi.org/10.1007/s11182-011-9658-4.

[22] P. Hazra, D. Chakrabarty, A. Chakraborty, N. Sarkar, Intramolecular charge transfer and solvation dynamics of Nile Red in the nanocavity of cyclodextrins, Chem. Phys. Lett. 388 (2004) 150–157, http://dx.doi.org/10.1016/j.cplett.2004.02.078.

[23] L.J. Magid, K. Konno, C.A. Martin, Binding of phenols to inverted micelles and microemulsion aggregates, J. Phys. Chem. 85 (1981) 1434–1439, http://dx.doi.org/10.1021/j150610a031.

[24] C. Comuzzi, P. Polese, A. Melchior, R. Portanova, M. Tolazzi, SOLVERSTAT: a new utility for multipurpose analysis. An application to the investigation of dioxygenated Co(II) complex formation in dimethylsulfoxide solution, Talanta 59 (2003) 67–80.

[25] P.J. Huber, Robust estimation of a location parameter, Ann. Math. Stat. 35 (1964) 73–101.

[26] M. Merli, L. Sciascia, M.L. Turco Liveri, Regression diagnostics applied in kinetic data processing: outlier recognition and robust weighting procedures, Int. J. Chem. Kinet. 42 (2010) 587–607, http://dx.doi.org/10.1002/kin.20510.

[27] D.A. Belsley, E. Welsch, R.E. Kuh, Regression Diagnostics: Identifying Influential Data and Sources of Collinearity, Wiley, New York, 1980 (u.a.).